Title
Non-lithographic SERS Substrates: Tailoring Surface Chemistry for Au Nanoparticle Cluster Assembly

Journal
Small, 8(14)

ISSN
1613-6810

Authors
Adams, Sarah M
Campione, Salvatore
Caldwell, Joshua D
et al.

Publication Date
2012-07-23

DOI
10.1002/smll.201102708

small
NANO MICRO

Non-lithographic SERS Substrates: Tailoring Surface Chemistry for Au Nanoparticle Cluster Assembly

*Sarah M. Adams, Salvatore Campione, Joshua D. Caldwell, Francisco J. Bezares, James C. Culbertson, Filippo Capolino, and Regina Ragan**

***N**ear-field plasmonic coupling and local field enhancement in metal nanoarchitectures, such as arrangements of nanoparticle clusters, have application in many technologies from medical diagnostics, solar cells, to sensors. Although nanoparticle-based cluster assemblies have exhibited signal enhancements in surface-enhanced Raman scattering (SERS) sensors, it is challenging to achieve high reproducibility in SERS response using low-cost fabrication methods. Here an innovative method is developed for fabricating self-organized clusters of metal nanoparticles on diblock copolymer thin films as SERS-active structures. Monodisperse, colloidal gold nanoparticles are attached via a crosslinking reaction on self-organized chemically functionalized poly(methyl methacrylate) domains on polystyrene-block-poly(methyl methacrylate) templates. Thereby nanoparticle clusters with sub-10-nanometer interparticle spacing are achieved. Varying the molar concentration of functional chemical groups and crosslinking agent during the assembly process is found to affect the agglomeration of Au nanoparticles into clusters. Samples with a high surface coverage of nanoparticle cluster assemblies yield relative enhancement factors on the order of 10^9 while simultaneously producing uniform signal enhancements in point-to-point measurements across each sample. High enhancement factors are associated with the narrow gap between nanoparticles assembled in clusters in full-wave electromagnetic simulations. Reusability for small-molecule detection is also demonstrated. Thus it is shown that the combination of high signal enhancement and reproducibility is achievable using a completely non-lithographic fabrication process, thereby producing SERS substrates having high performance at low cost.*

S. M. Adams, Prof. R. Ragan
Department of Chemical Engineering
and Materials Science
University of California
Irvine, Irvine, CA 92697, USA
E-mail: rragan@uci.edu

S. Campione, Prof. F. Capolino
Department of Electrical Engineering and Computer Science
University of California
Irvine, Irvine, CA 92697, USA

Dr. J. D. Caldwell, Dr. F. J. Bezares, Dr. J. C. Culbertson
Naval Research Laboratory
4555 Overlook Ave, S.W. Washington, DC 20375, USA

DOI: 10.1002/smll.201102708

1. Introduction

Planar assemblies of nanometer-spaced metal nanoparticles allow scientists and engineers to harness electromagnetic fields for imaging, photonics, and medicine at the nm-size scale. For instance, imaging at resolutions well below the diffraction limit is possible using 2D arrays of metal nanoparticles,[1] while photovoltaic devices have exhibited an increase in efficiency due to optical field enhancements associated with excitation of the surface plasmon resonance of metal nanoparticle arrays on the surface.[2] Planar nanoparticle arrays for medical diagnostics have achieved detection of target biomolecules at molecular concentrations significantly lower than conventional methods provide.[3] Studies

measuring signal enhancements in surface enhanced Raman scattering (SERS) sensors based on metal nanoparticles have shown that decreasing interparticle spacing between the metallic nanostructures yields exponential increases in signal intensity with the strongest electromagnetic signals being formed at hotspots between the nanoparticle with gaps below 10 nm.[4] It is also important to note that in creating such near-field plasmonically coupled systems, that the plasmonic fields induced are extended into the volume between the particles as opposed to being confined to the surface of an isolated particle. Au-coated polymer nanopillars fabricated using nanoimprint lithography from electron beam lithography-fabricated silicon molds were also used to create high enhancement factors when exposure to solvent caused the pillars to coalesce into pentagons with narrow gap spacings.[5] Facsimiles of Au nanoparticle aggregate-like clusters, prepared with conventional lithographic techniques exhibited $1–5 \times 10^8$ signal enhancement.[6] The development of low-cost non-lithographic methods for designing planar metal nanoarchitectures with nanometer scale interparticle spacing allows for greater utilization of the near-field properties in metal nanostructures for device applications. For example, colloid monolayers of Au and Ag nanoparticles measure 10^4 to 10^5 SERS signal enhancement,[7] and some have reported combined electromagnetic and chemical enhancements up to 10^7 when analytes chemically interact with nanoparticles.[8] Efforts to increase this enhancement with clusters of tightly spaced nanoparticles are of interest.

While low-cost SERS substrates have been realized, these frequently exhibit a wide distribution of SERS enhancement factors across a given sample surface. While conventional lithographic patterns have demonstrated uniform large-area (~100 μm or more) SERS at 1.2×10^8 signal enhancement with Au-capped nanopillars,[6b] and non-conventional lithographic methods such as Au deposition on anodized aluminum oxide substrates[9] with enhancements of 8×10^6 demonstrate less than 10% variance in sample signal uniformity, analysis of hexagonally closed packed (HCP) nanospheres coated with Ag determined that the hottest sites, local enhancement factor greater than 10^9, contributed to 24% of overall SERS intensity yet were distributed across only 0.006% of the total sample surface.[10] Other work involving HCP nanoparticles for SERS have reported enhancements of $10^4–10^7$.[11] Submonolayer coverage of Ag nanoparticles on surfaces also produces enhancements on the order of 10^7.[12] Efforts to produce SERS substrates with nanosphere lithography that produces metal triangular[13] or hexagonal cavity arrays,[14] have exhibited 10^6 to 10^8 SERS enhancements albeit there can exist difficulty in achieving high uniformity over large length scales. Wrinkled nanowalls with narrow gaps of gold films[15] have impressive signal enhancements, though exhibit one or two order of magnitude variability of SERS intensity in point-to-point measurements. Efforts to regulate SERS intensity uniformity across samples using hexagonally ordered Ag nanocap arrays[16] or by regulating hotspots on multi-tiered particle design[17] have produced patterns with theoretically calculated enhancement factors between 10^4 to 10^7 using finite-difference time-domain analysis. While it is difficult to directly compare enhancements in different systems, most non-lithographic SERS substrate designs exhibit signal variability due to non-uniformities on the substrate surface. Here we present a low-cost, self-organization method, for forming nanoparticle clusters over large areas in order to achieve uniform, large signal enhancements across the surface with the capability for reuse in small-molecule SERS detection.

The SERS substrates discussed here consist of arrays of nanoparticle clusters that are fabricated in the absence of any lithography and without the need for any vacuum phase metal deposition methods. To achieve nanometer scale interparticle distances to enable the generation of large volumes of SERS hotspots, colloidal nanoparticles were selectively attached on chemically functionalized self-organized domains on diblock copolymer surfaces[18] to form clusters. Prior work using self-organized diblock copolymers as templates produced composite Au-polymer nanopillars with feature sizes down to 100 nm,[19] arrays of single 10–40 nm Au nanoparticles[19,20] and Au/TiO_2 nanoparticles.[21] SERS substrates designed using diblock copolymer templates where Ag or Au was deposited on plasma or chemically etched nanopillar arrays produced signal enhancements up to 10^6.[22] Nanoparticles have also been electrostatically assembled on chemical domains with feature sizes as low as 100 nm that were patterned with soft UV nanoimprint lithography to produce amino terminated Si.[23] Here we use phase-separated polystyrene-*b*-poly(methyl methacrylate) (PS-*b*-PMMA) diblock copolymer thin films to achieve 40 nm poly(methyl methacrylate) (PMMA) domains that are chemically modified with primary amines[24] for controlled placement of carboxylic acid functionalized metal nanoparticles of monodisperse size and shape as small as 10 nm in diameter and achieved enhancements on the order of 10^9. It was found that by encasing the plasmonically active nanoparticles with thioctic acid ligands, the Au nanoparticles are both attached onto the PMMA chemical domains and are protected from further chemical bond formation on the surface. Thus, the sensor can be reused, as the analyte cannot chemically bond to the gold colloid. Prior work on reusable SERS sensors has involved more complicated surface chemical functionalization, such as approaches using reversible binding of an analyte with DNA aptamers.[25] Thioctic acid, with chain length of approximately 1 nm, functionalization is a facile approach to enable sensor reusability for Raman-active molecules.

The developed chemical self-assembly process also provides a platform with great versatility for metal nanoarchitecture design. Since the attachment mechanism involves the localized attachment of Au nanoparticles with thioctic acid ligands from colloids, the advantage of this method is the ability to attach any metallic nanostructures that can be functionalized with carboxylic ligands in colloidal solution. Nanoparticles prepared from colloidal solution can be produced with diverse size,[26] shape,[27] and core–shell composition[28] in order to tune its corresponding surface plasmon resonance.[29] Thus metal nanostructures with desired physical characteristics can be implemented onto a patterned template design. The diblock copolymer templates can be varied by simple changes in the polymer molecular weight[30] and interfacial

small 2012,
DOI: 10.1002/smll.201102708

small NANO MICRO

energy between template and substrate[31] to vary template patterns and thereby the arrangement of nanoparticles on surfaces. Furthermore, the copolymer matrix allows for incorporation of functional polymers designed as a diffusive trap for an analyte of interest[32] and uniform films have been fabricated on 3–8 inch wafers[33] that can be used to produce large area SERS sensors. Overall, this report presents how metal nanoparticle arrays can be varied by simple changes in the chemical design parameters to optimize nanoparticle spacing and cluster arrangements.

2. Results and Discussion

2.1. Chemical Assembly of Au Nanoparticles on Polymer Templates

Selective placement of Au nanoparticles on diblock copolymer templates is performed by selective chemical functionalization of PMMA domains on PS-*b*-PMMA thin films and chemical attachment of Au nanoparticles to PMMA domains. The process is depicted in the schematic in **Figure 1**. First, colloidal Au nanoparticles were functionalized by solution-phase ligand attachment of thioctic acid molecules that have carboxylic acid end groups, as illustrated in Figure 1a. Afterwards, PS-*b*-PMMA diblock copolymer thin films were immersed in an ethylenediamine/dimethylsulfoxide (ED/DMSO) solution to functionalize PMMA domains with surface primary amine chemical groups,[24] as shown in Figure 1b. 1-Ethyl-3-[3-dimethylaminopropyl] carbodiimide hydrochloride (EDC), via coordination cross-linking chemistry with *N*-hydroxysulfosuccinimide (S-NHS), was then used to anchor the Au nanoparticles onto PMMA domains.[18,34] EDC/S-NHS cross-linking chemistry is incorporated to facilitate bonding of Au colloidal nanoparticles with carboxyl ligands onto the amine-functionalized PMMA domains. A schematic of the reaction pathway is shown in Figure 1c, which is designed to lead to attachment of Au nanoparticles onto the PMMA domains as illustrated in Figure 1d.

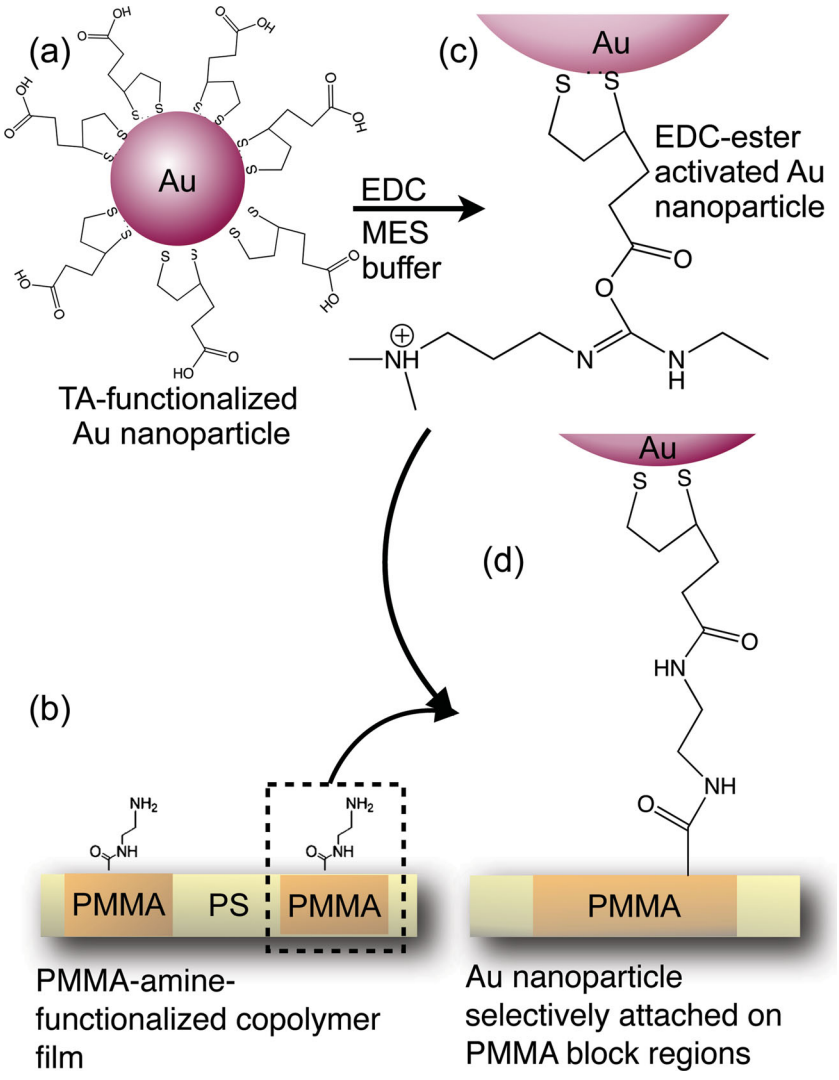

Figure 1. Schematic illustration of Au nanoparticle attachment on planar PS-*b*-PMMA thin film by a) surface chemistry functionalization of Au nanoparticles with thioctic acid and b) PMMA surface regions of copolymer with ethylenediamine, followed by c) EDC/S-NHS crosslinking chemistry on the nanoparticle, d) to selectively attach on the PMMA surface regions.

Citrate-stabilized Au nanoparticles in aqueous solutions were functionalized with thioctic acid ligand groups by addition of thioctic acid to solution. Dynamic light scattering (DLS) was used to measure nanoparticle size before and after the addition of thioctic acid (TA). Two sets of particles were analyzed, one set with diameter of 10 nm and the other set with diameter of 20 nm. DLS data of measured nanoparticle size versus molar concentration of thioctic acid within Au nanoparticle solution is presented in Supporting Information (SI), Figure S1. TA addition of 0.25 mM to aqueous nanoparticle solutions exhibited an increase in nanoparticle diameter in DLS measurements indicative of ligand attachment on the nanoparticle surface without aggregation. The addition of TA in concentrations greater than 0.5 mM for 10 nm nanoparticles and 1 mM for 20 nm nanoparticles exhibited an increased polydispersity index (PDI) in DLS measurements due to nanoparticle aggregation in solution. Thus, nanoparticles were functionalized with 0.25 mM unless otherwise indicated.

The PS-*b*-PMMA diblock copolymers used have number average molecular weight (M_n) of 260 kg mol^{-1} (PS) and 63.5 kg mol^{-1} (PMMA) and the resulting thin films have 40 nm diameter PMMA domains as measured by AFM. PS-*b*-PMMA diblock copolymers in toluene solution were spin-coated on Si(001) substrates with random PS/PMMA brush layer and annealed at 170 °C in order to initiate phase separation into PS and PMMA domains.[35] Though the work here was performed on Si(001) substrates, PS-*b*-PMMA diblock

DOI: 10.1002/smll.201102708

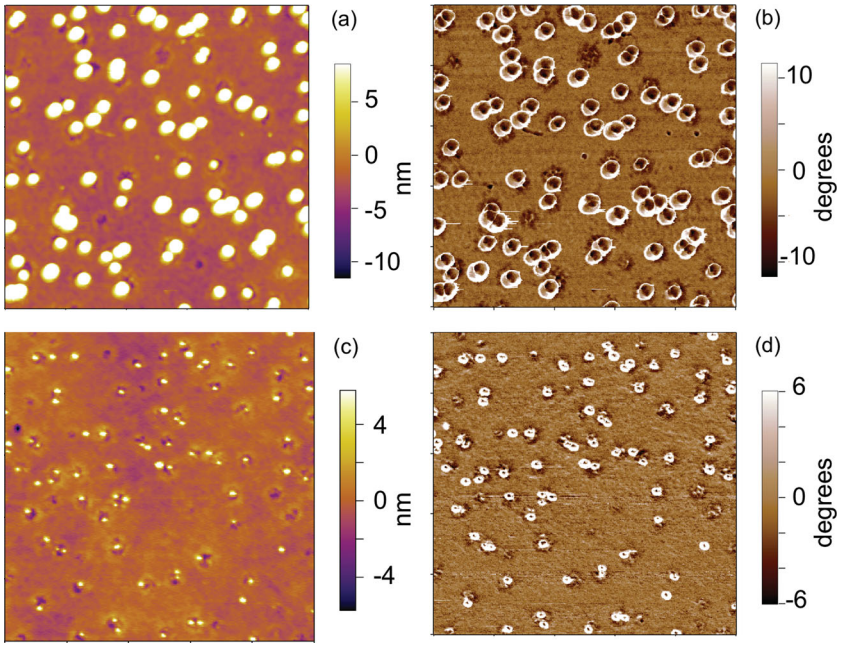

Figure 2. 1 μm × 1 μm AFM images of Au nanoparticles deposited on PS-*b*-PMMA thin films having M_n of 260 kg mol^{-1} (PS) and 63.5 kg mol^{-1} (PMMA) of a) topography and b) phase contrast with deposited 20 nm Au nanoparticles and of c) topography and d) phase contrast with deposited 10 nm Au nanoparticles.

copolymer thin films can also be formed on glass and plastic substrates.[36] PS-*b*-PMMA templates were immersed in ED/DMSO for 2 min at a concentration of 3% (v/v) of ethylenediamine in ED/DMSO.

The Au nanoparticle solution was treated with the EDC/S-NHS chemical crosslinker at concentrations of 30 μM EDC and 75 μM S-NHS for the 20 nm Au nanoparticles and at concentrations of 18 μM EDC and 45 μM S-NHS nanoparticle solution for the 10 nm Au nanoparticles while the substrate was immersed in the solution. In **Figure 2**, 1 μm × 1 μm AFM images showing topography (a) and phase contrast (b) are shown of Au nanoparticles having diameter of 20 nm and topography (c) and phase contrast (d) of Au nanoparticles having diameter of 10 nm that were chemically assembled on PS-*b*-PMMA templates. The AFM topography images presented in Figure 2a and d show the Au nanoparticles attach to depressed regions on the surface. Prior work has shown that ED/DMSO exposure of the PS-*b*-PMMA results in local depressions in PMMA domains.[18] In order to confirm the depressed regions are composed of PMMA, AFM phase images were also acquired. Phase imaging measures energy dissipation during tip approach and retraction.[37] Thus, PS and PMMA regions can be differentiated in AFM phase images since PMMA has a greater elastic modulus than PS and will appear darker in AFM phase imaging in repulsive mode thus, providing a method for evaluating nanoparticle selectivity for PMMA versus PS surface regions. In the phase images of Figure 2b and d, Au nanoparticles are observed on or adjacent to PMMA domains on the surface. This is consistent with previous studies for selective attachment of Au nanoparticles onto PMMA domains using EDC/S-NHS crosslinking chemistry.[18] It was also found in this prior study that in the absence of the crosslinking agent, only a few Au nanoparticles/μm^2 were observed on the surface.

In the AFM images of Figure 2, the surfaces are covered with several isolated Au nanoparticles, some dimers and a few trimers. We found the degree of clustering of Au nanoparticles chemically assembled on PMMA domains was affected by the molar concentration of thioctic acid for ligand attachment to Au nanoparticles, and the molar concentration of the EDC crosslinking agent. Three different samples were prepared for SERS analysis, all consisting of 20 nm Au nanoparticles on PS-*b*-PMMA templates with 40 nm PMMA domains, in order to investigate how the degree of Au nanoparticle clustering affects SERS response. AFM and SEM images were acquired to measure how cluster geometry was affected by varying chemical processing parameters. **Table 1** lists the process parameters that were varied and the resulting percentage of clusters containing multiple Au nanoparticles and the total Au nanoparticle coverage on the surface as determined from SEM images. At least ten SEM images with a field of view on the order of a few microns were analyzed for each sample to gather statistics on the surface coverage of cluster assemblies. The first sample was prepared with a reduced concentration of the EDC/S-NHS chemical crosslinker, 20 μM, in order to obtain a sample with primarily isolated nanoparticles. This sample had 16% of the nanoparticles on the surface incorporated into clusters and is referred to as 16MP; the rest are isolated nanoparticles on the surface. For the second sample, ligand attachment on Au nanoparticles was performed with thioctic acid concentration of 0.25 mM and 30 μM of EDC was used for crosslinking, the same process used for chemical assembly of Au nanoparticles described in the prior section and shown in Figure 2. This also produces predominantly single Au nanoparticles on the surface as observed in SEM analysis with 28% of the nanoparticles on the surface incorporated into clusters. This sample is referred to as 28MP. In order to increase Au nanoparticle agglomeration to achieve clusters with multiple nanopartices on the surface, the concentration of thioctic acid during ligand attachment was increased to 1.0 mM for the third sample while EDC concentration was held fixed. SEM analysis determined

Table 1. Sample process parameters for SERS analysis.

Sample no.	Sample name	Muliparticle frequency [%]	[Thioctic acid] [mM]	[EDC]-[S-NHS] [μM] - [μM]	Au areal coverage [%]
I	16MP	16 ± 8	0.25	20–50	3.2
II	28MP	28 ± 10	0.25	30–75	4.6
III	90MP	90 ± 5	1.0	30–75	15.4

small 2012,
DOI: 10.1002/smll.201102708

small NANO MICRO

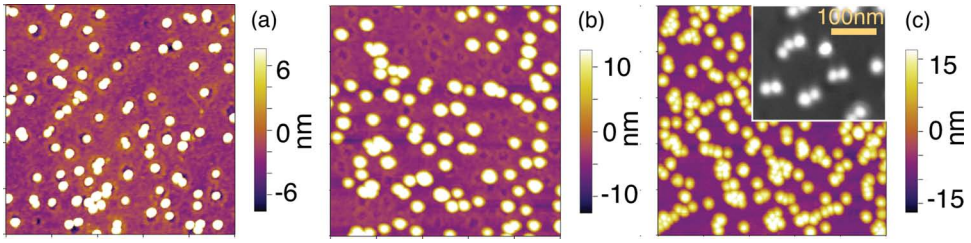

Figure 3. 1 μm × 1 μm AFM topography images of the nanoparticle-copolymer surfaces, 20 nm Au nanoparticles attached on 40 nm PMMA domains with varying nanoparticle clustering at a) 16% multi-particle clusters b) 28% multi-particle clusters, and c) 90% multi-particle clusters with SEM inset. As larger clusters form, Au nanoparticles extend to the PS regions on the surface.

that 90% of the nanoparticles are incorporated in clusters. This third sample is referred to as 90MP. AFM topography images are shown in **Figure 3**a, b, and c for the 16MP, 28MP, and 90MP samples, respectively, which demonstrate consistent particle height indicative of particle agglomeration as surface clusters instead of aggregation in the colloid.

2.2. SERS Measurements of Nanoparticle Arrays

SERS experiments were performed using a DeltaNu ExamineR micro-Raman system. Samples for SERS analysis were prepared by immersing PS-*b*-PMMA templates with Au nanoparticles in a 1mM solution of benzenethiol in ethanol for approximately 18 h. Measurements were collected from three separate lasers with excitation wavelengths of 532 nm, 633 nm, and 785 nm, focused to an approximately 2 μm spot size on the sample surface. The dominant observed SERS vibrational modes for benzenethiol and corresponding Raman shifts are labeled as ν_1 to ν_6 and shown in **Table 2**.[38] According to Mie theory, 20 nm Au nanoparticles have a surface plasmon resonance (SPR) near 533 nm. Thus, in the absence of plasmonic coupling, we expect the measured SERS intensities to be highest at 532 nm. However, the influence of the increased dielectric medium of PS and PMMA with respect to air and the interparticle plasmonic coupling induced due to their partial to almost complete agglomeration within the samples studied will induce a significant red shift in the SPR position.[39] Therefore, it was anticipated that SERS measurements near 532 nm incident would be relatively weak, with a stronger SERS response observed at 633 nm laser excitation with a drop-off in intensity when measured with 785 nm incident. As anticipated using a 532 nm excitation source, the SERS intensity was in the noise range for samples 16MP and 28MP and showed measurable intensity only for sample 90MP. A SERS spectrum is shown in the SI (Figure S2) for sample 90MP for 532 nm laser excitation. **Figure 4**a, b and c show SERS spectra with the intensity normalized for both the incident laser power and integration time for samples a) 16MP, b) 28MP, and c) 90MP at excitation wavelengths of 633 (dashed line) and 785 (solid line). The measured SERS intensity with the

Table 2. SERS spectral and assignments for benzenethiol.

Vibrational mode	Raman shift [cm^{-1}]	SERS assignments[a)]	Vibrational assignments[b)]
ν_1	420	7a(a_1), $\nu_{CS} + \beta_{CCC}$	C-S stretching and ring in-plane deformation
ν_2	690	6a(a_1), $\beta_{CCC} + \nu_{CS}$	Ring in-plane deformation and C-S stretching
ν_3	998	12(a_1), β_{CCC}	Ring out-of-plane deformation and C-H out-of-plane bending
ν_4	1021	18a(a_1), β_{CH}	Ring in-plane deformation and C-C symmetric stretching
ν_5	1071	1(a_1), $\beta_{CCC} + \nu_{CS}$	C-C symmetric stretching and C-S stretching
ν_6	1571	8a(a_1), ν_{CC}	C-C symmetric stretching

[a)]Taken from Reference [38a]. Letters in parentheses indicate vibrational symmetry, while β and ν indicate in-plane bending and stretching modes, respectively; [b)]Taken from Reference [38b].

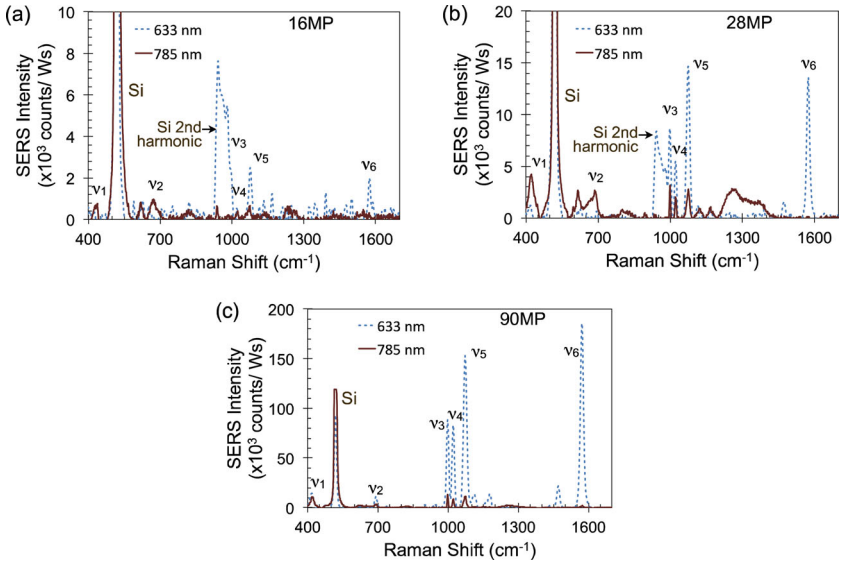

Figure 4. SERS spectra recorded from three separate samples of 20 nm Au attached on 40 nm PMMA regions of PS-*b*-PMMA thin film treated with a monolayer of benzenethiol for optical enhancement analysis comparing signal measured with change in excitation laser wavelength of 633 nm and 785 nm for a) 16MP, b) 28MP, and c) 90MP. SERS vibrational peaks ν_1-ν_5 are identified in Table 2.

DOI: 10.1002/smll.201102708

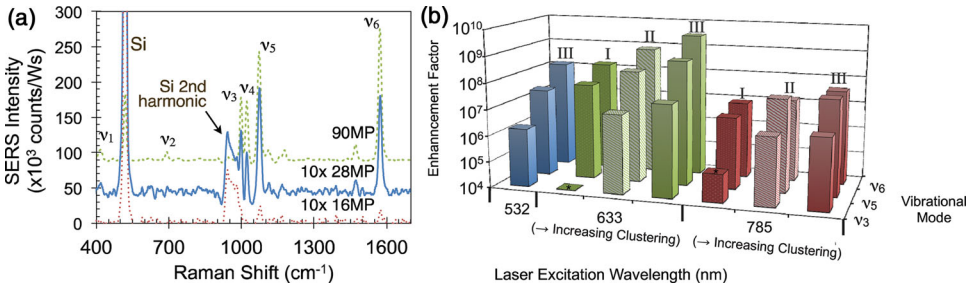

Figure 5. a) SERS spectra obtained at 633 nm laser excitation from 16% MP, 28% MP, and 90% MP samples. b) SERS signal enhancement factors (EF) are graphed comparing laser excitation wavelength at 532, 633, and 785 nm for vibrational peaks ν_3, ν_5, and ν_6 for 16MP, 28MP, and 16MP. ($*\nu_3$ data for 16MP was poorly distinguishable from 2nd Si harmonic peak.)

633 nm excitation laser is clearly stronger for all designated vibrational peaks, thus the SERS enhancement was maximum near this incident wavelength. This implies that consistent with the hypothesis outlined above, that the SPR for the collections of Au nanoparticles within these samples is located near 633 nm, with the center presumably located to the red of this wavelength, thus explaining the stronger SERS response at 785 nm with respect to 532 nm incident.

2.2.1. SERS Signal Enhancement Factor Analysis

We compare the SERS spectra obtained at 633 nm for the three different samples. In **Figure 5**a, SERS spectra for 16MP, 28MP, and 90MP samples demonstrate significant increase in SERS signal with increased nanoparticle coverage and multiparticle clustering. It is significant to note that the Au areal coverage of 16MP and 28MP does not greatly differ; the difference is less than 1.5%. Yet the SERS signal is much lower for 16MP than 28MP illustrating the importance of plasmonic coupling between nanoparticles that occurs due to the nanoparticle agglomeration to achieve high enhancement values. In order to quantify, the Raman enhancement factor (EF) was calculated for the ν_3 vibrational mode at 998 cm^{-1} for all three samples from the expression:

$$EF = \frac{I_{SERS}/N_{SERS}}{I_{Raman}/N_{Raman}} \quad (1)$$

where I_{SERS}, I_{Raman}, N_{SERS}, and N_{Raman} are the SERS and neat Raman intensities and number of molecules measured, respectively. In this calculation,

$$I_{SERS} = I_{Raw}^{SERS}/(P \cdot t) \quad (2)$$

is the measured SERS signal normalized for laser power (P) and acquisition time (t).

$$N_{SERS} = \rho_{surf} N_A \left(f_{Au} A_{spot}\right) \quad (3)$$

is the average number of absorbed molecules in the laser stimulated SERS region. This value is determined by normalizing the excited surface area with the Au area coverage percentage, which when combined with the reported surface coverage of benzenethiol ρ_{surf} of 0.544 nmol/cm^2,[6b,40] provides an accurate measurement of the number of molecules participating in the SERS measurement. Further, N_A is Avogadro's number, f_{Au} is the Au nanoparticle fractional coverage, and A_{spot} of the laser spot size area. I_{Raman} is the Raman signal intensity in solution phase (Neat) of the measured analyte benzenethiol molecule again normalized for laser power and acquisition time, for which $N_{Raman} = \rho_{neat} V$ is the average number of molecules in a scattering volume V with benzenethiol density ρ_{neat} of 9.739 mmol/cm^3.[6b] In the calculation of EF, we normalize with the Au nanoparticle coverage in order to directly compare samples. The ν_3 mode at 998 cm^{-1} was used for the EF since this mode has the strongest Raman signal for neat benzenethiol.

The average calculated EF at the ν_3 SERS vibrational mode was $1.0 \times 10^7 \pm 0.3 \times 10^7$ (1σ) for the 28MP sample and $3.1 \times 10^7 \pm 0.9 \times 10^7$ (1σ) EF for the 90MP sample. Note that the 16MP SERS signal at the ν_3 (998 cm^{-1}) peak was poorly distinguishable from the Si second harmonic vibrational peak and thus an EF could not be accurately calculated. The largest EF calculated for 90MP was 4.1×10^7. This is several orders of magnitude greater than the SERS enhancement of roughened Au surface under optimal conditions.[41] We also consistently see the same order of magnitude enhancement from sample to sample. The relative SERS EF increases approximately by a factor of 5 when comparing the EF ratio of 28MP to 16MP and approximately by a factor of 4 when comparing the EF ratio of 90MP to 28MP. Thus, agglomeration of Au nanoparticles into multi-particle clusters leads to higher EF due to the significantly larger plasmonic electromagnetic field intensities induced via plasmonic coupling. In order to compare SERS enhancements for all samples, relative EF calculations were also performed using Equation 1 for addition vibrational modes of benzenethiol, ν_5 and ν_6.

Figure 5b summarizes the EF and the relative EF that were calculated for all samples, in Table 1, as a function of the laser excitation wavelength (532, 633, and 785 nm) and vibrational mode. As mentioned prior, only the 90MP sample produced sufficient SERS signal when excited at 532 nm and thus the other samples are not plotted at this wavelength. Figure 5b shows that for all samples and all the vibrational modes, excitation at 633 nm produced SERS EF that are one to two orders of magnitude greater than those calculated from resulting data at the 532 nm and 785 nm excitation laser sources. The 90MP sample exhibits enhancements of $3.1 \times 10^7 \pm 0.9 \times 10^7$ (1σ), $5.8 \times 10^8 \pm 1.4 \times 10^8$ (1σ), $3.1 \times 10^9 \pm 0.8 \times 10^9$ (1σ) for ν_3, ν_5, and ν_6, respectively. In the SI, we provide the details of the calculation of EF and show the detailed calculation for the ν_6 mode for the 90MP sample.

small 2012,
DOI: 10.1002/smll.201102708

NANO MICRO small

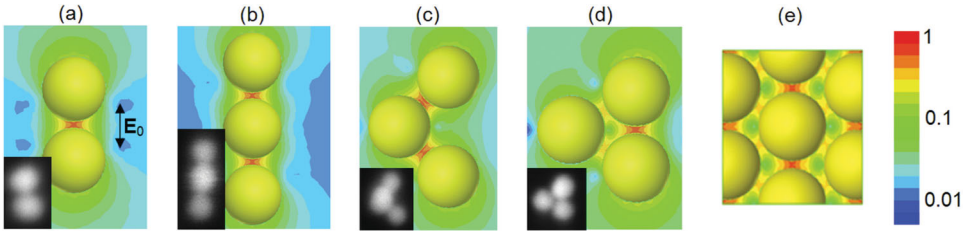

Figure 6. Normalized field map for different configurations: a) dimers, b) linear trimers, c) trimers (90°), d) trimers (60°), and e) hexagonal close-packed (HCP). All field maps have been computed with plane wave illumination with electric field polarized as in (a). Values of field enhancement factor are in Table 3.

Table 3. Electric field enhancement E_{cl}/E_0 for different cluster configurations. The SERS enhancement is proportional to the fourth power of the field enhancement.

Wavelength [nm]	Dimers	Linear trimers	Trimers (60°)[a)]	Trimers (90°)[a)]	HCP[a)]
532	17.4	15.7	16.6/ 13.8	12.9/ 13.5	8.1/ 7.5
633	62.9	89.7	49.7/ 45.4	58.1/ 32.6	23.8/ 20
785	20	25.8	17.2/ 15.4	16.5/ 11.8	25/ 24.4

[a)]For the trimers (60° and 90°) and the HCP cases, the '/'symbol separates enhancements for vertical (as in Figure 6) and horizontal polarized incident electric field, respectively.

Full-wave simulations using HFSS[42] of representative metal clusters fabricated in this paper (shown as insets in **Figure 6**): dimers, linear trimers, trimers (60°), and trimers (90°), are performed, and a summary of the results is shown in **Table 3** and Figure 6. For comparison purposes, we analyze also the standard hexagonal close-packed (HCP) configuration. The aim of the numerical simulations is to show the formation of field hot spots, and thus the field enhancement, intended as E_{cl}/E_0, where E_0 is the plane wave field magnitude without clusters and E_{cl} is the maximum field magnitude with clusters, occurring between the nanospheres. Au nanoparticles in simulations have diameter of 23 nm, in agreement with dynamic light scattering measurements of nanoparticle diameters (with permittivity matching the values from[43]). The nanospheres have been assumed to be embedded in a layer with dielectric constant of 2.47 (40 nm thickness) which accounts for the PMMA layer with a homogeneous layer of molecules on top, on top of a silicon substrate. The gap between the nanospheres is assumed to be 2 nm taken from SEM images and used in HCP structures for accurate comparison. For simplicity of calculations we assume that the clusters in Figure 6 are arrayed in a square lattice, with a period large enough to affect weakly the maximum field between the nanospheres in a cluster (in Table 3 the assumed period is 120 nm; see SI (Table S1) for results assuming a period of 150 nm that do not show a dependence between field and periodicity). We illuminate each structure with a plane wave orthogonal to the surface and polarized as in Figure 6a at the three laser wavelengths employed in the experiment (i.e., 532, 633 and 785 nm): the field enhancement results are summarized in Table 3. The data leads to two-main observations: i) stronger field enhancement is achieved at 633 nm laser excitation, in agreement with the experimental results in Figure 5; and ii) stronger field enhancement is achieved with the dimer and trimer clusters analyzed in this paper with respect to a HCP configuration, at 633 and 532 nm. This is due, in part, to the fact that the HCP array exhibits a red shifted resonance with respect to dimers and trimers. At 785 nm, the HCP exhibits a field enhancement stronger than or equal to the one of the clusters at the same wavelength, that is still however lower than the field enhancement of dimers and trimers at 633 nm. These results show that ad-hoc clusters can be designed and fabricated to obtain larger field enhancements than with the HCP structure for the particle dimensions considered in this paper. Ordered periodic structures may exhibit large enhancements also due to long-range interactions and this depends on the complex resonance frequency or wavenumber evaluated as in Fructos et al.,[44] for example. Also breaking of local symmetry may excite dark modes,[45] not considered here, that may lead to strong enhancements as well. More precise assessments considering also ordering as well as other particle dimensions and distances require further investigation. Since the fabrication process developed allows for nanoparticle diameter and shape to be varied, simulations can provide insight for optimal structures.

In Figure 6 we show the normalized field maps (with respect to each maximum field magnitude) for the structures analyzed in Table 3 with 633 nm laser excitation, exhibiting the expected hot spots between the nanoparticles. As a final remark, the SERS enhancement is proportional to the fourth power of the field enhancements shown in Table 3. For example, the linear trimer at 633 nm exhibits a $E_{cl}/E_0 = 6.5 \times 10^7$ enhancement, purely looking at the field, which is however smaller than the value of 10^9 shown in Figure 5. This difference is expected because in the calculation we have completely neglected any molecule-cluster near-field interaction, which is supposed to further enhance scattering. Accurate investigations accounting for such interactions will be carried out in the future, for example simulations that include an ideal dipole in the gap between nanoparticles yield higher enhancements than those in Table 3.

Furthermore, a uniform SERS response was reproducibly observed across the sample surface for both 90MP and 28MP. In **Figure 7**a and b, the measured SERS spectra with modes ν_3, ν_4, and ν_5 labeled are shown for multiple positions on sample 28MP and 90MP, respectively. The signal is relatively consistent from point to point on the surface, as observed in the standard deviation values, indicating that hotspots are distributed across the surface and uniform with respect to the laser spot size. By increasing the areal coverage of Au on the surface beyond 15%, and thereby the density of hotspots

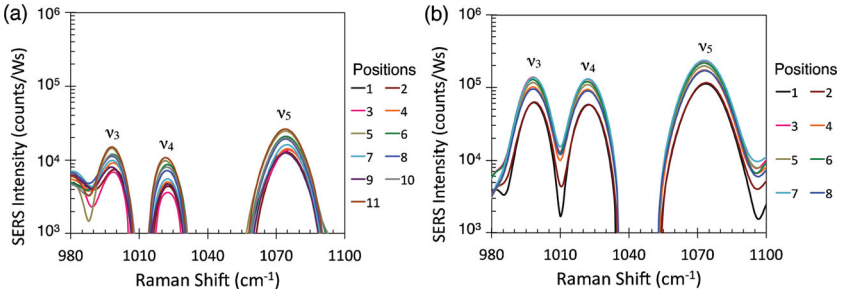

Figure 7. SERS intensity measurements at multiple sample positions for ν_3, ν_4, and ν_5 vibrational peaks for a) 28MP and b) 90MP.

in the laser spot, we expect a reduction in acquisition time below the current 30 s. Self-assembled SERS substrates to date have exhibited a high degree of variability in signal response across a single sample surface; EF typically vary by a few orders of magnitude[10,15] and typically require longer acquisition times.

2.2.2. Nanoparticle Array Reusability and Shelf Life

Reusability and shelf life of the SERS substrates was also examined. Following the initial SERS analysis at 785 nm laser excitation, data shown in (Figure 4), 16MP, 28MP and 90MP, within three days of the initial exposure and measurement, no longer exhibited benzenethiol related SERS intensity when excited at 785 nm. These samples were analyzed again with three different SERS deposition and measurement cycles of varying excitation wavelength six months later after re-exposure to benzenethiol, providing seven separate measurements of reusability. SERS measurements acquired at 785 nm laser excitation were analyzed immediately after re-exposure and again seven days later. In **Figure 8**a, SERS measurements with 785 nm laser excitation for sample 28MP are shown i) after the initial exposure, ii) immediately after benzenethiol re-exposure six months after the initial exposure, and iii) seven days after the re-exposure without any further treatment or rinsing of the sample. Immediately after benzenethiol re-exposure, case (ii), the samples clearly displayed renewed SERS signal strength at approximately 25% the original measurement for 28MP when comparing the ν_3, ν_4, and ν_5 vibrational modes. SERS intensity associated with ν_3, ν_4, and ν_5 vibrational modes are not observable seven days later, case (iii), suggesting that the benzenethiol has evaporated from the surface and thus did not chemically bind to the gold nanoparticles, illustrating the protective nature of the thioctic acid surface treatment. We therefore attribute the ability to re-use samples to the fact that thioctic acid is stable on the Au nanoparticle surface and is not exchanged with the benzenethiol analyte. Small or bulky incoming ligands are sterically hindered from replacing the original ligand monolayer on the nanoparticle surface.[46] Therefore, while the molecular analyte of interest during SERS analysis can approach the plasmonic fields needed to induce the SERS effect, the sensor can be reused, as the analyte cannot chemically bond to Au nanoparticles. Renewed SERS intensity at ν_3, ν_4, and ν_5 after re-exposure to benzenethiol solution [case (ii)] indicates that the benzenethiol molecule is absorbed on the polymer surface and held in regions near the Au nanoparticles. In Figure 8b, SERS measurements were performed on i) 90MP, ii) 28MP, and iii) 16MP after a second benzenethiol exposure that occurred 6 months after the initial exposure. Although the SERS signal strength is not always equal to the original measured signal, it is stronger on samples with higher Au nanoparticle clusters, and the benzenethiol SERS vibrational modes are detectible on all three samples. This indicates the potential viability of fabricating reusable SERS substrates, with analyte removal between analyses, even for analytes with a strong chemical affinity for the Au nanoparticles. Further, by modifying the nanoparticle material, size, shape and density one can envision fabricating tailored SERS substrates for a given incident wavelength with low cost, highly reproducible methods.

3. Conclusion

To summarize, thioctic-acid functionalized Au nanoparticles were preferentially attached onto the ethylenediamine-modified PMMA regions of PS-*b*-PMMA diblock copolymer templates when using EDC/S-NHS as a chemical crosslinker. The agglomeration of Au nanoparticles into clusters is dependent on the concentration of the chemical cross-linking agent and the concentration of thioctic-acid during nanoparticle functionalization. For samples with a higher fraction of Au nanoparticles incorporated in clusters, this SERS-substrate fabrication method provides reproducibly high enhancement factors across the sample surface. For instance, comparing the response at 633 nm excitation for the ν_6 mode, the average EF measured on the surface was 3.1×10^9 for a sample with a high fractional coverage of clusters (90MP) and lower, 7.6×10^8, for a sample with a lower fractional coverage of clusters

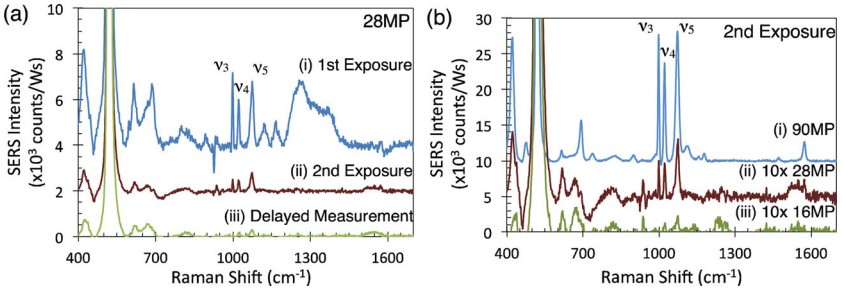

Figure 8. SERS spectra obtained at 785 nm laser excitation from samples with benzenethiol vibrational peaks ν_3, ν_4, and ν_5 designated for: a) sample with 28MP coverage with benzenethiol monolayer deposited on the surface including scan of i) 1st exposure, ii) after benzenethiol 2nd re-exposure, and iii) following a 7-day delay after exposure and b) samples measured after redeposition of benzenethiol with MP coverage of i) 90MP, ii) 28MP, and iii) 16MP.

small 2012,
DOI: 10.1002/smll.201102708

NANO MICRO small

(28MP), i.e., more isolated single particles. The self-organized chemical domains on the diblock copolymer surface and nanoparticle chemical attachment on domains allow for formation of clusters on surfaces with narrow gap spacing. Full-wave HFSS simulations of the local field enhancement as a function of cluster arrangement demonstrate that high signal enhancements are associated with the narrow gap spacing in the different types of clusters observed in SEM data. These simulations show that at 633 nm excitationlinear clusters provide maximum signal enhancement with dimers and trimers being only slightly lower. The EF is maximum at 633 nm for cluster arrangements in agreement with experimental results. SERS signal intensity for the detection of benzenethiol was uniform when comparing measurements taken across a single sample surface for the two samples, 28MP and 90MP. In the case of benzenethiol detection, the SERS-active molecule is volatile and removable in between measurements becausethe thioctic acid is not exchanged during the measurement, providing reusability for an unmodified SERS spectra with respect to the Raman spectra of the analyte molecule. Removal of larger analyte molecules may be possible via rinsing allowing for multiple applications. This method also exhibits versatility in nanostructure surface array formation, whereby we demonstrated array assembly of spherical nanoparticles down to 10 nm in diameter, the chemical methods used could be applied to nanoparticles and nanorods of many different sizes, shapes, and compositions. Overall, the fabrication method thus provides the capacity for creating reproducible and reusable SERS-active surfaces with a high degree of versatility in architecture, and thereby SPR frequency, using inexpensive materials and self-assembly processes.

4. Experimental Section

Materials: Random copolymer poly(styrene-*co*-methyl methacrylate)-α-hydroxyl-ω-tempo moiety (PS-*r*-PMMA) (M_n = 7400, 59.6% PS) and block copolymer poly(styrene-*b*-methyl methacrylate) (PS-*b*-PMMA) (M_n = 260 000 (PS), 63 500 (PMMA)) were purchased from Polymer Source, Inc. (Dorval, Canada). Gold(III) chloridetrihydrate($HAuCl_4 \cdot 3H_2O$), DL-6,8-thioctic acid ($C_8H_{14}O_2S_2$), ethylenediamine, dimethyl sulfoxide (DMSO), ethanol, isopropanol, and toluene were purchased from Sigma Aldrich (St. Louis, MO). Sodium citrate, sodium hydroxide, hydrofluoric acid (HF) were purchased from Fisher Scientific (Pittsburgh, PA). MES 0.1 M buffer, 1-ethyl-3-[3-dimethylaminopropyl] carbodiimide hydrochloride (EDC), and *N*-hydroxy sulfosuccinimide (S-NHS) were purchased from Thermo Scientific Pierce Protein Research Products (Rockford, IL). Silicon (110) wafers were purchased from University Wafer (South Boston, MA). Nanopure water (18.2 MΩ cm^{-1}) was obtained from a Milli-Q Millipore System and used for all experiments.

Nanoparticle Preparation and Functionalization: Two sets of Au nanoparticles were prepared for chemical attachment on the copolymer surface, one by sodium citrate stabilization in aqueous colloidal solution (1 wt%) at 20 nm diameter and the second as purchased from British Biocell International in aqueous colloid (1 wt%) at 10 nm diameter. The nanoparticle size was verified by measurement with dynamic light scattering using a Zetasizer Nano ZS. The two nanoparticle sets were treated identically with the attachment of carboxylic acid ligand groups. The nanoparticles were first washed once, replacing the solvent with dilute pH 11.67 NaOH solution, followed by chemical ligand functionalization with DL-6,8-thioctic acid (Sigma-aldrich) with 18 h continuous stirring, as described in previous research.[18] A range of thioctic acid concentration (5 to 20 µL, 0.05 mM) in ethanol for each milliliter of Au nanoparticle solution was analyzed. For the experimental standard of TA (0.25 µM) in Au nanoparticle solutions were prepared by the addition of TA in ethanol (5 µL, 0.05 mM) to the aqueous Au nanoparticle solution. After attachment, the residual thioctic acid was removed and the basicity of the colloidal solution was reduced to pH 8 by centrifuging the 20 nm Au-TA nanoparticles at 7000 *g* for 20 min and the 10 nm Au-TA at 65 000 *g* for 50 min followed by resuspension of the nanoparticles in Milli-pore MilliQ deionized water.

Patterned Copolymer Template Preparation and Functionalization: The diblock copolymer patterned thin films were formed on flat silicon substrates by spin coat deposition of block copolymer solution in toluene. To form vertical arrangement of the copolymer block domains on the substrates, random copolymer brush was formed such that the polymer domains have a neutral interface wetting to the substrate and orient perpendicular to the substrate.[47] For this, a random PS-r-PMMA, with anchoring α-hydroxy-ω-tempo moiety end groups, was deposited on the substrates, which were cleaned beforehand and treated with a fresh oxide layer for the Si substrate. The random copolymer, having number average molar mass (M_n) and weight average molar mass (M_w) of 7.4 kg mol^{-1} and 11.8 kg mol^{-1}, was deposited to form a thin film by spin coating a toluene solution (1 wt%) at 3000 rpm for 45 s. The film was annealed at 170 °C for 72 h in vacuum conditions, followed by rinsing with toluene to form a 6–7 nm film with random patterning 59.6% surface polystyrene.

PS-*b*-PMMA diblock copolymer template was then formed on the prepared random copolymer layer with molecular weight 260 kg mol^{-1} (PS) and 63.5 kg mol^{-1} (PMMA). Polymer solution of 1 wt% in toluene was deposited from spin-coat deposition on the random copolymer surfaces at 5000 rpm for 45 s. The resulting thin film was annealed at 170 °C for 120 h.

The PMMA regions of the diblock copolymer were functionalized with primary amine surface end groups by treatment with dilute ethylenediamine.[24] The polymer films were immersed in solutions of ethylenediamine in dimethylsulfoxide (2% v/v), where the length of time treated effected marginal polymer surface etching from 1 to 5 min. The surfaces were then rinsed with isopropanol before further treatment.

Nanoparticle Crosslinking Attachment: The thioctic acid-functionalized nanoparticles are attached onto the ethylenediamine-functionalized PMMA surface domains of the diblock copolymer templates by the interaction of an EDC/S-NHS chemical crosslinker. The crosslinker is introduced by the addition of an EDC (2 mM) and a S-NHS (5 mM) solution in MES buffer (0.1 M) to the aqueous TA-functionalized nanoparticle colloidal solution. The volume of the crosslinker solution (5 to 20 µL) was varied per milliliter of Au colloid depending on the resultant interparticle clustering desired. The amine-functionalized polymer films were then suspended in the solution, and incubated at 40 °C for 1-h durations followed by isopropanol wash.

Nanocharacterization: The surfaces were analyzed with atomic force microscopy using an Asylum Research MFP 3D atomic force

DOI: 10.1002/smll.201102708

microscope (AFM) with 75 kHz resonance frequency AFM probes with diamond-like carbon coating produced by BudgetSensors. Scanning electron microscopy (SEM) analysis was measured with an Ultra 55 scanning electron microscopy (Carl Zeiss, Germany), a Sirion XL30 SFEG (FEI, Hillsboro, USA) and a NovaLab200 Dual Beam SEM (FEI).

SERS: To measure the Raman signal for examining SERS enhancement, the arrays were immersed in a 10^{-3} M solution of benzenethiol in ethanol for 18 h to form a molecular monolayer. SERS measurements were carried out using a DeltaNu ExamineR micro-Raman system, in which a 532, 633, or 785 nm laser was focused on an approximately 2 μm spot on the sample surface, and Raman spectra was collected in back reflection geometry through the 50× 0.7 NA objective and was focused onto a thermo-electrically cooled CCD array, with laser power varied from 0.5 to 40 mW and acquisition time of 30 s (633 and 785 nm) and 60 s (532 nm).

Supporting Information

Supporting Information is available from the Wiley Online Library or from the author.

Acknowledgements

The authors acknowledge the National Science Foundation CHE-0748912 and CMMI- 1101074 for funding this work. The authors acknowledge the use of the facilities within the Carl Zeiss Center of Excellence at the University of California, Irvine and the DeltaNu Raman system at Howard University. The authors also thank Ansys for providing HFSS that was instrumental in this work.

[1] a) P. Alitalo, C. Simovski, A. Viitanen, S. Tretyakov, *Phys. Rev. B* **2006**, *74*, 235425; b) J. B. Pendry, *Phys. Rev. Lett.* **2000**, *85*, 3966–3969.

[2] a) B. P. Rand, P. Peumans, S. R. Forrest, *J. Appl. Phys.* **2004**, *96*, 7519–7526; b) S. Pillai, K. R. Catchpole, T. Trupke, M. A. Green, *J. Appl. Phys.* **2007**, *101*, 093105; c) D. M. Schaadt, B. Feng, E. T. Yu, *Appl. Phys. Lett.* **2005**, *86*, 063106.

[3] a) N. Nath, A. Chilkoti, *Anal. Chem.* **2001**, *74*, 504–509; b) A. J. Haes, R. P. V. Duyne, *Expert Rev. Mol. Diagn.* **2004**, *4*, 527–537.

[4] a) J. J. Shiang, J. R. Heath, C. P. Collier, R. J. Saykally, *J. Phys. Chem. B* **1998**, *102*, 3425–3430; b) K. H. Su, Q. H. Wei, X. Zhang, J. J. Mock, D. R. Smith, S. Schultz, *Nano Lett.* **2003**, *3*, 1087–1090; c) J. D. Caldwell, O. J. Glembocki, F. J. Bezares, M. I. Kariniemi, J. T. Niinistö, T. T. Hatanpää, R. W. Rendell, M. Ukaegbu, M. K. Ritala, S. M. Prokes, C. M. Hosten, M. A. Leskelä, R. Kasica, *Opt. Express* **2011**, *19*, 26056–26064; d) P. J. Schuck, D. P. Fromm, A. Sundaramurthy, G. S. Kino, W. E. Moerner, *Phys. Rev. Lett.* **2005**, *94*, 017402.

[5] F. S. Ou, M. Hu, I. Naumov, A. Kim, W. Wu, A. M. Bratkovsky, X. Li, R. S. Williams, Z. Li, *Nano Lett.* **2011**, *11*, 2538–2542.

[6] a) S. M. Wells, S. D. Retterer, J. M. Oran, M. J. Sepaniak, *ACS Nano* **2009**, *3*, 3845–3853; b) J. D. Caldwell, O. Glembocki, F. J. Bezares, N. D. Bassim, R. W. Rendell, M. Feygelson, M. Ukaegbu, R. Kasica, L. Shirey, C. Hosten, *ACS Nano* **2011**, *5*, 4046–4055.

[7] a) K. C. Grabar, R. G. Freeman, M. B. Hommer, M. J. Natan, *Anal. Chem.* **1995**, *67*, 735–743; b) R. G. Freeman, K. C. Grabar, K. J. Allison, R. M. Bright, J. A. Davis, A. P. Guthrie, M. B. Hommer, M. A. Jackson, P. C. Smith, D. G. Walter, M. J. Natan, *Science* **1995**, *267*, 1629–1632; c) Z. Zhu, T. Zhu, Z. Liu, *Nanotechnology* **2004**, *15*, 357.

[8] F. Toderas, M. Baia, L. Baia, S. Astilean, *Nanotechnology* **2007**, *18*, 255702.

[9] D. Choi, Y. Choi, S. Hong, T. Kang, L. P. Lee, *Small* **2010**, *6*, 1741–1744.

[10] Y. Fang, N.-H. Seong, D. D. Dlott, *Science* **2008**, *321*, 388–392.

[11] a) A. Wei, *Chem. Commun.* **2006**, 1581–1591; b) A. Kaminska, O. Inya-Agha, R. J. Forster, T. E. Keyes, *Phys. Chem. Chem. Phys.* **2008**, *10*, 4172–4180; c) Y. Wang, H. Chen, E. Wang, *Nanotechnology* **2008**, *19*, 105604; d) H. Y. Jung, Y.-K. Park, S. Park, S. K. Kim, *Anal. Chim. Acta* **2007**, *602*, 236–243.

[12] Y. Han, R. Lupitskyy, T.-M. Chou, C. M. Stafford, H. Du, S. Sukhishvili, *Anal. Chem.* **2011**, *83*, 5873–5880.

[13] C. L. Haynes, R. P. Van Duyne, *J. Phys. Chem. B* **2003**, *107*, 7426–7433.

[14] a) S. Mahajan, M. Abdelsalam, Y. Suguwara, S. Cintra, A. Russell, J. Baumberg, P. Bartlett, *Phys. Chem. Chem. Phys.* **2007**, *9*, 104–109; b) S. Cintra, M. E. Abdelsalam, P. N. Bartlett, J. J. Baumberg, T. A. Kelf, Y. Sugawara, A. E. Russell, *Faraday Discuss.* **2006**, *132*, 191–199.

[15] L. Zhang, X. Lang, A. Hirata, M. Chen, *ACS Nano* **2011**, *5*, 4407–4413.

[16] T. Qiu, W. Zhang, X. Lang, Y. Zhou, T. Cui, P. K. Chu, *Small* **2009**, *5*, 2333–2337.

[17] J.-S. Wi, S. Sengupta, R. J. Wilson, M. Zhang, M. Tang, S. X. Wang, *Small* **2011**, *7*, 3276–3280.

[18] J. H. Choi, S. M. Adams, R. Ragan, *Nanotechnology* **2009**, *20*, 065301.

[19] W. Zou, Y. Wang, Z. Wang, A. Zhou, J. Li, A. Chang, Q. Wang, M. Komura, K. Ito, T. Iyoda, *Nanotechnology* **2011**, *22*, 335301.

[20] M. Aizawa, J. M. Buriak, *J. Am. Chem. Soc.* **2005**, *127*, 8932–8933.

[21] J. Polleux, M. Rasp, I. Louban, N. Plath, A. Feldhoff, J. P. Spatz, *ACS Nano* **2011**, *5*, 6355–6364.

[22] a) J. Lu, D. Chamberlin, D. A. Rider, M. Liu, I. Manners, T. P. Russell, *Nanotechnology* **2006**, *17*, 5792; b) Y. Wang, M. Becker, L. Wang, J. Liu, R. Scholz, J. Peng, U. Gösele, S. Christiansen, D. H. Kim, M. Steinhart, *Nano Lett.* **2009**, *9*, 2384–2389.

[23] S. Gilles, C. Kaulen, M. Pabst, U. Simon, A. Offenhäusser, D. Mayer, *Nanotechnology* **2011**, *22*, 295301.

[24] L. Brown, T. Koerner, J. H. Horton, R. D. Oleschuk, *Lab Chip* **2006**, *6*, 66–73.

[25] N. H. Kim, S. J. Lee, M. Moskovits, *Adv. Mater.* **2011**, *23*, 4152–4156.

[26] a) T. S. Ahmadi, Z. L. Wang, T. C. Green, A. Henglein, M. A. ElSayed, *Science* **1996**, *272*, 1924–1926; b) M. C. Daniel, D. Astruc, *Chem. Rev.* **2004**, *104*, 293–346.

[27] a) S. E. Skrabalak, L. Au, X. Li, Y. Xia, *Nat. Protoc.* **2007**, *2*, 2182–2190; b) H. Chen, X. Kou, Z. Yang, W. Ni, J. Wang, *Langmuir* **2008**, *24*, 5233–5237.

[28] S. J. Oldenburg, R. D. Averitt, S. L. Westcott, N. J. Halas, *Chem. Phys. Lett.* **1998**, *288*, 243–247.

[29] a) S. Schultz, D. R. Smith, J. J. Mock, D. A. Schultz, *Proc. Natl. Acad. Sci. USA* **2000**, *97*, 996–1001; b) K. L. Kelly, E. Coronado, L. L. Zhao, G. C. Schatz, *J. Phys. Chem. B* **2002**, *107*, 668–677; c) J. J. Mock, M. Barbic, D. R. Smith, D. A. Schultz, S. Schultz, *J. Chem. Phys.* **2002**, *116*, 6755–6759; d) P. Albella, B. Garcia-Cueto, F. González, F. Moreno, P. C. Wu, T.-H. Kim, A. Brown, Y. Yang, H. O. Everitt, G. Videen, *Nano Lett.* **2011**, *11*, 3531–3537.

[30] T. Xu, H.-C. Kim, J. DeRouchey, C. Seney, C. Levesque, P. Martin, C. M. Stafford, T. P. Russell, *Polymer* **2001**, *42*, 9091–9095.

[31] a) E. Han, K. O. Stuen, M. Leolukman, C.-C. Liu, P. F. Nealey, P. Gopalan, *Macromolecules* **2009**, *42*, 4896–4901; b) D. Y. Ryu,

DOI: 10.1002/smll.201102708

S. Ham, E. Kim, U. Jeong, C. J. Hawker, T. P. Russell, *Macromolecules* **2009**, *42*, 4902–4906.
[32] B. A. Higgins, D. L. Simonson, E. J. Houser, J. G. Kohl, R. A. McGill, *J. Polym. Sci., Part A: Polym. Chem.* **2010**, *48*, 3000–3009.
[33] a) K. W. Guarini, C. T. Black, Y. Zhang, H. Kim, E. M. Sikorski, I. V. Babich, *J. Vac. Sci. Technol., B* **2002**, *20*, 2788–2792; b) M. Park, C. Harrison, P. M. Chaikin, R. A. Register, D. H. Adamson, *Science* **1997**, *276*, 1401–1404.
[34] Z. Grabarek, J. Gergely, *Anal. Biochem.* **1990**, *185*, 131–135.
[35] C. T. Black, K. W. Guarini, *J. Polym. Sci., Part A: Polym. Chem.* **2004**, *42*, 1970–1975.
[36] X. Jiang, H. Zheng, S. Gourdin, P. T. Hammond, *Langmuir* **2002**, *18*, 2607–2615.
[37] a) B. Anczykowski, B. Gotsmann, H. Fuchs, J. P. Cleveland, V. B. Elings, *Appl. Surf. Sci.* **1999**, *140*, 376–382; b) R. García, A. San Paulo, *Phys. Rev. B* **1999**, *60*, 4961–4967.
[38] a) T. H. Joo, M. S. Kim, K. Kim, *J. Raman Spectrosc.* **1987**, *18*, 57–60; b) S. Li, D. Wu, X. Xu, R. Gu, *J. Raman Spectrosc.* **2007**, *38*, 1436–1443.
[39] C. G. Blatchford, J. R. Campbell, J. A. Creighton, *Surf. Sci.* **1982**, *120*, 435–455.
[40] J. Y. Gui, D. A. Stern, D. G. Frank, F. Lu, D. C. Zapien, A. T. Hubbard, *Langmuir* **1991**, *7*, 955–963.
[41] C. C. Busby, J. A. Creighton, *J. Electroanal. Chem.* **1982**, *140*, 379–390.
[42] Finite element based simulation software by Ansys, http://www.ansoft.com/products/hf/hfss/(last accessed March **2012**)
[43] P. B. Johnson, R. W. Christy, *Phys. Rev. B* **1972**, *6*, 4370–4379.
[44] A. L. Fructos, S. Campione, F. Capolino, F. Mesa, *J. Opt. Soc. Am. B* **2011**, *28*, 1446–1458.
[45] J. A. Fan, K. Bao, C. Wu, J. Bao, R. Bardhan, N. J. Halas, V. N. Manoharan, G. Shvets, P. Nordlander, F. Capasso, *Nano Lett.* **2010**, *10*, 4680–4685.
[46] A. C. Templeton, W. P. Wuelfing, R. W. Murray, *Acc. Chem. Res.* **1999**, *33*, 27–36.
[47] a) P. Mansky, Y. Liu, E. Huang, T. P. Russell, C. Hawker, *Science* **1997**, *275*, 1458–1460; b) P. Mansky, T. P. Russell, C. J. Hawker, M. Pitsikalis, J. Mays, *Macromolecules* **1997**, *30*, 6810–6813.

Received: December 22, 2011
Revised: March 13, 2012
Published online: